

Precession–tracking coordinates for simulations of compact–object–binaries

Serguei Ossokine,^{1,2} Lawrence E. Kidder,³ and Harald P. Pfeiffer^{1,4}

¹*Canadian Institute for Theoretical Astrophysics, University of Toronto, Toronto, Ontario M5S 3H8, Canada*

²*Department of Astronomy and Astrophysics, University of Toronto, Toronto, Ontario M5P 3H4, Canada*

³*Center for Radiophysics and Space Research, Cornell University, Ithaca, New York, 14853*

⁴*Fellow, Canadian Institute for Advanced Research*

(Dated: October 1, 2018)

Binary black hole simulations with black hole excision using spectral methods require a coordinate transformation into a co-rotating coordinate system where the black holes are essentially at rest. This paper presents and discusses two coordinate transformations that are applicable to *precessing* binary systems, one based on Euler angles, the other on quaternions. Both approaches are found to work well for binaries with moderate precession, i.e. for cases where the orientation of the orbital plane changes by $\ll 90^\circ$. For strong precession, performance of the Euler-angle parameterization deteriorates, eventually failing for a 90° change in orientation because of singularities in the parameterization (“gimbal lock”). In contrast, the quaternion representation is invariant under an overall rotation, and handles any orientation of the orbital plane as well as the Euler-angle technique handles non-precessing binaries.

PACS numbers: 04.25.D-, 04.25.dg, 04.25.Nx, 04.30.-w

I. INTRODUCTION

Gravitational waves offer an exciting new observational window into the universe. With the second generation of gravitational wave detectors such as Advanced LIGO and Advanced Virgo commencing observations in 2015 [1], it is extremely important to develop a detailed picture of the gravitational physics of the most likely sources. A very promising source of gravitational waves are inspiraling and merging binary black holes [2]. Because of the weakness of the gravitational wave signal, matched filtering is necessary to pick out the waveform from the noise [3, 4]. Constructing such templates, in turn, requires direct numerical integration of Einstein’s equations for the late inspiral, merger and ringdown phase of the coalescing compact object binary; see, e.g. [5]. Since 2005, starting with the seminal work of Frans Pretorius [6], many groups have successfully simulated binary black hole systems using a variety of different techniques. For recent overviews of the state of the field, see [7, 8].

Compact object inspirals fall into two categories: non-precessing and precessing. While the non-precessing aligned-spin systems arguably represent an important subspace of all binary black hole systems, the more general case features arbitrary spin orientations. In this non-symmetric situation, the interaction of the orbital angular momentum and the black holes’ spins leads to precession of the orbital plane, changing its orientation by as much as 180 degrees.

Precession modulates the gravitational waveform. Therefore, it is crucial to explore these strongly precessing systems. Furthermore, precessing systems allow the study of gravitational dynamics in an underexplored regime, providing a new opportunity for comparing numerical relativity to various analytic approximations like post-Newtonian (see e.g. [9, 10]) and effective-one-body theory (see e.g. [11–14]). The numerical simulations can

be used both to test the accuracy of the analytic treatments and to calibrate them, in some cases, thus improving their accuracy [15–17]. Furthermore, one can attempt to reproduce numerically predictions from analytic computations such as transitional precession [18], which is known from PN theory but has not yet been observed in numerical simulations.

Numerical simulations of precessing binary black holes have already been undertaken; for example [19–26]. Given the vastness of parameter space and the need for simulations lasting at least 10 orbits - possibly 100’s of orbits - to optimally exploit gravitational wave detectors [5, 27–31], a lot of extra work remains to be done.

The Spectral Einstein Code SpEC [32] allows efficient and accurate simulations of binary black holes; see e.g. [31, 33–39]. This code applies black hole excision and uses time-dependent coordinate mappings to rotate and deform the computational grid such that the excision regions remain inside the black hole horizons at all times. For non-precessing inspiralling binaries, these coordinate mappings are described in detail in previous work [33, 36, 40].

The purpose of the present paper is to develop coordinate mappings that are able to follow a precessing compact object binary through the inspiral, even for strongly precessing systems. We present two different approaches. The first one is based on Euler angles; it works well for moderate precession, but fails when the orientation of the orbital plane changes by 90 degrees or more. The second approach is designed to avoid the deficiencies of the Euler angle parameterization. By using quaternions, we devise coordinate mappings that work for any change of orientation of the orbital plane with a performance comparable to the earlier non-precessing techniques. The techniques developed here have already been used in [41, 42]

This paper is organized as follows. Section II describes the computational setup of SpEC in more detail

(Sec. II A), and develops the coordinate mappings based on Euler angles (Sec. II B) and quaternions (Sec. II C). Section III presents a sequence of numerical results obtained with both approaches, starting from Newtonian and post-Newtonian test-cases to simulations of binary black holes with numerical relativity (NR). We summarize our results in Sec. IV.

II. METHODS AND TECHNIQUES

A. Dual frames and control systems

As described in Scheel et al. [43], SpEC utilizes a dual-frame approach to simulate compact object binaries. Einstein’s equations are written down in an asymptotically non-rotating coordinate-system $x^{\bar{a}} = (\bar{t}, x^{\bar{i}})$, referred to as the “inertial frame”, and all tensors are represented in the coordinate basis of this frame. In the inertial frame, tensor components remain finite even at large separation. The computational grid is specified in “grid coordinates” $x^a = (t, x^i)$. The collocation points of the spectral expansion are at constant grid coordinates, and numerical derivatives are computed with respect to these coordinates. The two coordinate frames share the same time-coordinate

$$\bar{t} = t. \quad (1)$$

The spatial coordinates of the two frames are related by a coordinate transformation

$$x^{\bar{i}} = x^{\bar{i}}(x^i; \lambda^\mu(t)), \quad (2)$$

which depends on a set of parameters $\lambda^\mu(t)$ to be discussed in detail later. The coordinate transformation Eq. (2) maps the grid-coordinates into the inertial frame such that the excision surfaces (coordinate spheres in the grid-frame) are mapped to locations somewhat inside the apparent horizons of the black holes in the inertial frame.

In the original work [43], this coordinate transformation was taken as the composition of a rotation about the z-axis and an overall scaling of the coordinates¹,

$$x^{\bar{i}} = \begin{pmatrix} \bar{x} \\ \bar{y} \\ \bar{z} \end{pmatrix} = a(t) \begin{pmatrix} \cos \psi(t) & -\sin \psi(t) & 0 \\ \sin \psi(t) & \cos \psi(t) & 0 \\ 0 & 0 & 1 \end{pmatrix} \begin{pmatrix} x \\ y \\ z \end{pmatrix}. \quad (3)$$

In this simple case, the map $\lambda^\mu(t) = \{a(t), \psi(t)\}$ depends on two parameters: the scale factor $a(t)$ and the rotation angle $\psi(t)$. The map parameters $\lambda^\mu(t)$ are chosen dynamically during the simulation, such that the map tracks the actual motion of the black holes. This can be accomplished by introducing a set of control-parameters Q^μ , such that

1. $Q^\mu = 0$ if the mapped excision spheres are at the desired location in inertial coordinates.
2. Under small variations of the mapping parameters around their current values, the control-errors satisfy

$$\left. \frac{\partial Q^\mu}{\partial \lambda^\nu} \right|_{\lambda^\mu = \lambda^\mu(t)} = -\delta_\nu^\mu \quad (4)$$

While not strictly required, Eq. (4) allows one to write down uncoupled feedback control equations for the $\lambda^\mu(t)$. In the special case of a linear, uncoupled system, this reduces to $Q^\mu = \lambda_{target}^\mu - \lambda^\mu$.

For black holes orbiting in the xy-plane, Eq. (3) suffices to keep the excision boundaries inside the inspiraling black holes, resulting in successful simulations of inspiraling BH–BH binaries in Ref. [44]. Subsequently, the map was refined to avoid a rapid inward motion of the outer boundary [34], to adjust the shapes of the mapped excision boundaries to more closely conform to the distorted apparent horizons [37, 38, 45], and was generalized to unequal mass binaries [36]. Hemberger et al [40] summarizes these maps, and introduces further mappings that are needed during the merger phase of the black hole binary.

The purpose of the present paper is the development of coordinate mappings that can handle precessing binaries. Because in general the center of mass will move (e.g due to asymmetric GW emission), these coordinate mappings must also allow for a translation of the binary. Rotation and translation couple to each other and must therefore be dealt with simultaneously. The questions addressed in this paper are therefore (1) determination of a suitable coordinate mapping for precessing, translating binaries, (2) suitable choice of mapping parameters λ^μ , and (3) derivation of control-parameters Q^μ . Specifically, we will discuss below two generalizations of Eq. (3), one based on Euler-angles and one based on quaternions. We will show that the Euler-angle representation suffers from singularities when the inclination of the orbital plane passes through $\pi/2$, and we will demonstrate that the quaternion representation fixes these problems.

B. Euler angle representation

In the general case where the orbital plane precesses, we use a mapping that composes a scaling $a(t)$, a rotation $R(t)$ and a translation $\vec{T}(t)$. The mapping is given by

$$\vec{x} = a(t) R(t) \vec{x} + \vec{T}. \quad (5)$$

A rotation matrix can be specified by Euler angles,

$$R = \begin{pmatrix} \cos \theta \cos \psi & -\cos \phi \sin \psi + \sin \phi \sin \theta \cos \psi & \sin \phi \sin \psi + \cos \phi \sin \theta \cos \psi \\ \cos \theta \sin \psi & \cos \phi \cos \psi + \sin \phi \sin \theta \sin \psi & -\sin \phi \cos \psi + \cos \phi \sin \theta \sin \psi \\ -\sin \theta & \sin \phi \cos \theta & \cos \phi \cos \theta \end{pmatrix}. \quad (6)$$

where ϕ is the roll angle around the x -axis, θ is the pitch angle around the y -axis, and ψ is the yaw angle around the z axis and we have suppressed the explicit time-dependence.

For our application, the desired locations of the black holes lie parallel to the x -axis, i.e. the black holes are at grid coordinates (c_A^x, c^y, c^z) and (c_B^x, c^y, c^z) . It is straightforward to show that for these two points a rotation about the x -axis is degenerate with a translation *because only the location of the black holes is important*. Therefore, we can set $\phi(t) = 0$ so that²

$$R = \begin{pmatrix} \cos \theta \cos \psi & -\sin \psi & \sin \theta \cos \psi \\ \cos \theta \sin \psi & \cos \psi & \sin \theta \sin \psi \\ -\sin \theta & 0 & \cos \theta \end{pmatrix}. \quad (7)$$

Thus the mapping in Eq. (5) will have six parameters in this case, a scaling $a(t)$, a pitch angle (rotation about y -axis) $\theta(t)$, a yaw angle (rotation about z -axis) $\psi(t)$, and a translation $(T^X(t), T^Y(t), T^Z(t))$.

The goal of the scaling-rotation-translation map is to keep the horizons of the two black holes centered on the excision surfaces. As the binary evolves, the map parameters need to be adjusted by the control system. To derive the control parameters Q^μ , c.f. Eq(4), one can consider perturbations of the mapping parameters around their current values. Let $\lambda^\mu = \{a, \theta, \psi, \vec{T} = (T^X, T^Y, T^Z)\}$ be the current imperfect mapping parameters at some time during the evolution. Furthermore, denote the desired parameters $\lambda_0^\mu = \lambda^\mu + \delta\lambda^\mu = \{a_0, \theta_0, \psi_0, T_0^X, T_0^Y, T_0^Z\}$. Finally, let \vec{x}_A and \vec{x}_B denote the current location of the center of black hole A and B, respectively³, and let \vec{c}_A and \vec{c}_B denote the desired location of the black hole centers; i.e., the centers of the excision spheres. For convenience we also define the vectors $\vec{X} = \vec{x}_A - \vec{x}_B$ and $\vec{C} = \vec{c}_A - \vec{c}_B$. The target mapping λ_0^μ is such that the points \vec{c}_A, \vec{c}_B are mapped onto the inertial frame position of the black holes, $\vec{c}_A = \vec{x}_A, \vec{c}_B = \vec{x}_B$:

$$\vec{x}_{A,B} = a_0 R(\theta_0, \psi_0) \vec{c}_{A,B} + \vec{T}_0. \quad (8)$$

Rewriting this equation in terms of the current mapping and the grid location of each black hole (i.e $\vec{x}_{A,B}$) yields

$$aR(\theta, \psi)\vec{x}_i + \vec{T} = (a + \delta a)R(\theta + \delta\theta, \psi + \delta\psi)\vec{c}_i + \vec{T} + \delta\vec{T}. \quad (9)$$

where $i = A, B$.

Equation (9) represents six equations for the six unknowns $\delta\lambda^\mu$. Solving this system of equations to leading order in the perturbations yields

$$\delta a = a \left(\frac{X^x}{C^x} - 1 \right), \quad (10a)$$

$$\delta\theta = \frac{-X^z}{C^x}, \quad (10b)$$

$$\delta\psi = \frac{1}{\cos \theta} \frac{X^y}{X^x}, \quad (10c)$$

$$\delta T^X = \frac{a}{C^x} (\delta t^X \cos \theta \cos \psi - \delta t^Y \sin \psi + \delta t^Z \sin \theta \cos \psi), \quad (10d)$$

$$\delta T^Y = \frac{a}{C^x} (\delta t^X \cos \theta \sin \psi + \delta t^Y \cos \psi + \delta t^Z \sin \theta \sin \psi), \quad (10e)$$

$$\delta T^Z = \frac{a}{C^x} (-\delta t^X \sin \theta + \delta t^Z \cos \theta) \quad (10f)$$

where

$$\delta t^X = c_A^x x_B - c_B^x x_A + c^y X^y + c^z X^z, \quad (11a)$$

$$\delta t^Y = c_A^x y_B - c_B^x y_A - c^y X^x - c^z X^y \tan \theta, \quad (11b)$$

$$\delta t^Z = c_A^x z_B - c_B^x z_A + c^y X^y \tan \theta + c^z X^x, \quad (11c)$$

Furthermore, we have assumed that the centers of the excision surfaces are aligned parallel to the x -axis so that $c_A^y = c_B^y = c^y$ and $c_A^z = c_B^z = c^z$.

Perhaps surprisingly, the $\delta\lambda^\mu$ given by Eq. (10a–10f) are the desired control parameters Q^μ . This can be seen as follows. For a perfect map, $\lambda^\mu = \lambda_0^\mu$, i.e. $\delta\lambda^\mu = Q^\mu = 0$. Moreover, by definition

$$\frac{\partial Q^\mu}{\partial \lambda^\nu} = \frac{\partial}{\partial \lambda^\nu} (\lambda_0^\mu - \lambda^\mu) = \frac{\partial \lambda_0^\mu}{\partial \lambda^\nu} - \frac{\partial \lambda^\mu}{\partial \lambda^\nu} = -\delta_\nu^\mu. \quad (12)$$

Thus $\delta\lambda^\mu$ defined by Eq. (10a–10f) satisfy the conditions for Q^μ outlined in section II A.

The Euler angle prescription as described above is adequate for describing rotations that are close to the $x-y$ plane, and has been used for the SpEC simulations presented in [45]. However, the Euler angle prescription carries with it an inherent coordinate singularity that causes

¹ Note that in Ref. [43], the equations give the transformation from the inertial coordinates to the grid coordinates, the rotation angle is ϕ instead of ψ , and the scale factor a is the inverse of the scale factor in this paper.

² Note that if the motion is confined to the $x-y$ plane, the pitch will remain fixed at $\theta = 0$ and we recover the rotation matrix in Eq. (3).

³ The precise definition of “center” is not important; we shall use the coordinate point around which the coordinate radius of the apparent horizon has vanishing $l = 1$ multipoles.

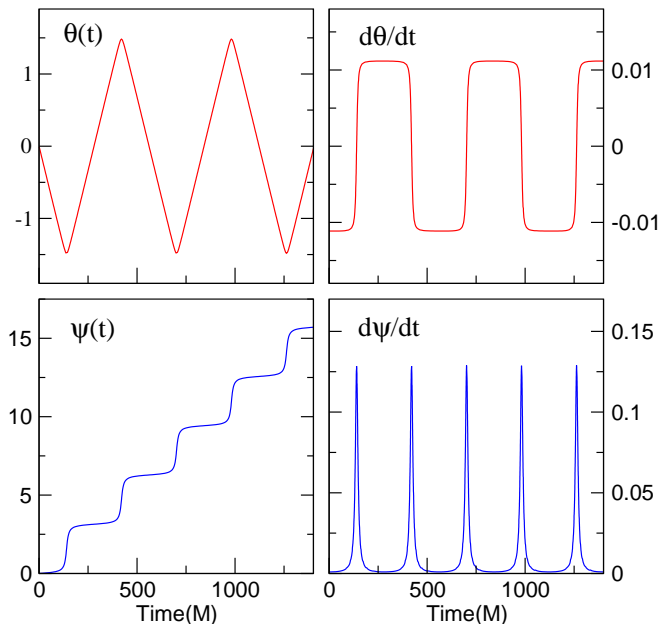


FIG. 1. Typical behaviour of the Euler angles and their derivatives for a nearly polar orbit inclined at 85 degrees with respect to the $x - y$ plane

a breakdown of the control system for high inclination angles. Firstly, note that Eq. (10c) shows that $\delta\psi$ will diverge when $\theta = \frac{\pi}{2}$, which would lead to the breakdown of a feedback control system. Further, since SpEC uses proportional-derivative-control or proportional-integral-derivative-control [40], we must examine the behaviour of the derivatives of the Euler angles, $\dot{\theta}$, $\dot{\psi}$. Notice that we can relate the angular velocity to the derivatives of the Euler angles simply by the relationship

$$(\omega_1, \omega_2, \omega_3)^T = A (\dot{\phi}, \dot{\theta}, \dot{\psi})^T, \quad (13)$$

where A is the Euler angle rates matrix:

$$A = \begin{pmatrix} \cos \psi \cos \theta & -\sin \psi & 0 \\ \sin \psi \cos \theta & \cos \psi & 0 \\ -\sin \theta & 0 & 1 \end{pmatrix}. \quad (14)$$

The black holes move on regular trajectories with a slowly varying orbital frequency $\bar{\omega}$ in inertial coordinates; therefore, the left-hand side of Eq. (13) is continuous. However, $|\det A| = |\cos(\theta)|$, so that for $\theta = \frac{\pi}{2}$ the time-derivatives of the Euler angles will diverge since, by Cramer's rule, the inverse of A scales as $1/\det A$.

There is another way to envision the divergence of the derivatives of the Euler angles. Consider the unit vector in the direction connecting the centers of the two compact objects in inertial coordinates, $\hat{u} = \frac{\vec{x}_B - \vec{x}_A}{|\vec{x}_B - \vec{x}_A|}$. Before, we considered ψ , θ as parameters in a mapping. Let us now consider them as spherical polar coordinates that

describe this vector⁴

$$\begin{pmatrix} u_x \\ u_y \\ u_z \end{pmatrix} = \begin{pmatrix} \cos \psi \cos \theta \\ \sin \psi \cos \theta \\ \sin \theta \end{pmatrix}. \quad (15)$$

We can immediately derive the expressions for $\dot{\theta}$, $\dot{\psi}$ as functions of \dot{u}_x , \dot{u}_y , \dot{u}_z :

$$\dot{\theta} = \frac{\dot{u}_z}{\cos \theta}, \quad (16)$$

$$\dot{\psi} = \frac{1}{\cos \theta} \sqrt{\dot{u}_x^2 + \dot{u}_y^2 - \dot{u}_z^2 \tan^2 \theta}. \quad (17)$$

From these equations it is obvious that the derivatives of θ and ψ behave abnormally when \hat{u} moves across one of the poles at uniform velocity. In fact, $\dot{\theta}$ does not exist, and its second derivative diverges (see the top panels of Fig. 1). Meanwhile, $\dot{\psi}$ diverges: letting $\delta\theta = \frac{\pi}{2} - \theta$ we can write, for $\delta\theta \ll 1$:

$$\dot{\psi} \propto \frac{\omega}{\delta\theta}. \quad (18)$$

This behaviour is demonstrated clearly in Figure 1, where the derivatives of both Euler angles demonstrate sharp and nearly discontinuous features.

This is the fundamental reason why Euler angles are not a suitable parametrization of rotations: there exist situations, which we would like to study, when their derivatives grow extremely fast numerically.

C. Rotation-invariant Quaternion representation

The origin of the break-down of the Euler angle representation lies in its reliance of a preferred coordinate system, which is implicit in the adoption of Euler angles. The physics of compact object inspirals is invariant under rotations of the spatial coordinates. Ideally, the numerical methods used to describe such a system should also be invariant, and should work equally well independent of the orbital plane of the black holes.

The singularities in the Euler angle representation arise from a poor choice of representation of the rotation group, which relied on preferred directions in space (namely the coordinate axes). Therefore, a suitable representation must be independent of any special directions. We employ quaternions to represent rotations and build up the overall rotation from a sequence of infinitesimal rotations.

It should be noted that a similar construction can be done with a different parametrization of rotations. See the Appendix for an example using orthogonal infinitesimal rotation matrices.

⁴ θ here means the angle to the xy plane rather than the angle to the z -axis. Therefore the following equations differ slightly from standard spherical polar coordinates.

1. Quaternion algebra

Quaternions are an extension of the complex numbers, with three imaginary units i, j , and k , obeying

$$i^2 = j^2 = k^2 = ijk = -1, \quad (19)$$

as well as certain further multiplication rules. A quaternion \mathbf{q} has the form

$$\mathbf{q} = q_0 + q_1i + q_2j + q_3k, \quad q_0, \dots, q_3 \in \mathbb{R} \quad (20)$$

This is conveniently written as $\mathbf{q} = (q_0, \vec{q})$, where $\vec{q} = (q_1, q_2, q_3)$. Addition and scalar multiplication are defined in analogy with complex numbers. With the structure introduced so far, the set of quaternions

$$\mathbb{H} = \{q_0 + q_1i + q_2j + q_3k | q_i \in \mathbb{R}\} \quad (21)$$

is a 4-dimensional vector space over the real numbers. Multiplication is defined by

$$\mathbf{qp} = (p_0q_0 - \vec{p} \cdot \vec{q}, p_0\vec{q} + q_0\vec{p} + \vec{p} \times \vec{q}), \quad (22)$$

where $\vec{q} \cdot \vec{q}$ and $\vec{q} \times \vec{p}$ are the standard Euclidean dot and cross products respectively. Complex conjugation is given by

$$\mathbf{q}^* = (q_0, -\vec{q}). \quad (23)$$

It follows that the multiplicative inverse is given by

$$\mathbf{q}^{-1} = \frac{\mathbf{q}^*}{|\mathbf{q}|}, \quad (24)$$

where the norm $|\mathbf{q}|$ satisfies

$$|\mathbf{q}|^2 = \mathbf{q} \mathbf{q}^* = q_0^2 + \vec{q}^2. \quad (25)$$

Restricting our attention now to the set of all unit quaternions $Sp(1) = \{\mathbf{q} \in \mathbb{H}, |\mathbf{q}| = 1\}$, it is easy to show that $Sp(1)$ is isomorphic to $SU(2)$ where $SU(2)$ is the group of all 2×2 unitary matrices with unit determinant [46]. $SU(2)$ is a double cover of the rotation group $SO(3)$, which means that unit quaternions do represent rotations.

Unit quaternions are related to rotations in the following manner. Let \hat{n} be a unit-vector, and define

$$\mathbf{q} = \left(\cos \frac{\theta}{2}, \hat{n} \sin \frac{\theta}{2} \right) \quad (26)$$

for some angle θ . The quaternion \mathbf{q} rotates a vector \vec{v} into the vector \vec{v}' , around the axis \hat{n} by angle θ in the right-handed sense via

$$\mathbf{v}' = \mathbf{q} \mathbf{v} \mathbf{q}^*. \quad (27)$$

In this equation, 3-vectors are to be promoted to quaternions by the rule $\mathbf{v} = (0, \vec{v})$, $\mathbf{v}' = (0, \vec{v}')$, and $|\mathbf{q}| = 1$

implies that \mathbf{v}' has indeed a vanishing real part. Equation (27) is equivalent to $\vec{v}' = R_{\mathbf{q}} \vec{v}$, with rotation matrix

$$R_{\mathbf{q}} = \begin{pmatrix} q_0^2 + 2q_1^2 - \vec{q}^2 & 2(q_1q_2 - q_0q_3) & 2(q_0q_2 + q_1q_3) \\ 2(q_1q_2 + q_0q_3) & q_0^2 + 2q_2^2 - \vec{q}^2 & 2(q_2q_3 - q_0q_1) \\ 2(q_1q_3 - q_0q_2) & 2(q_0q_1 + q_2q_3) & q_0^2 + 2q_3^2 - \vec{q}^2 \end{pmatrix} \quad (28)$$

We can now rewrite Eq. (5) in quaternion language,

$$\vec{x} = a \mathbf{q} \mathbf{x} \mathbf{q}^* + \mathbf{T}. \quad (29)$$

Here, $\vec{x}, \vec{x}, \vec{T}$ have been promoted to quaternions; e.g., $\mathbf{T} = (0, \vec{T})$.

Our next task is to derive equations that determine the time evolution of \mathbf{q} as well as the control parameters Q^μ .

2. Quaternion kinematics

In this section we derive the differential equation obeyed by the rotation quaternion \mathbf{q} . Consider a time-dependent unit-quaternion $\mathbf{q}(t) : \mathbb{R} \rightarrow Sp(1)$. The derivative is defined by

$$\dot{\mathbf{q}} = \lim_{h \rightarrow 0} \frac{\mathbf{q}(t+h) - \mathbf{q}(t)}{h} \quad (30)$$

We write the rotation $\mathbf{q}(t+h)$ at time $t+h$, as a product of $\mathbf{q}(t)$ and a quaternion \mathbf{u} representing an infinitesimal rotation,

$$\mathbf{q}(t+h) = \mathbf{u} \mathbf{q}(t). \quad (31)$$

The quaternion \mathbf{u} is easily obtained by expanding the right hand side of Eq. (26) to first order in θ using $\cos \frac{\theta}{2} \approx 1$, $\sin \frac{\theta}{2} \approx \frac{\theta}{2}$:

$$\mathbf{u} = \left(1, \hat{n} \frac{\theta}{2} \right) = 1 + \delta \mathbf{q} / 2 \quad (32)$$

with $\delta \mathbf{q} = (0, \hat{n}\theta)$. If the rotational velocity is $\vec{\omega}$ in inertial coordinates, then $\hat{n} = \hat{\omega}$ and $\delta\theta = \omega h$, so that $\delta \mathbf{q} = \omega h$. Thus we can write $\mathbf{q}(t+h) = (I + \delta \mathbf{q} / 2) \mathbf{q}(t)$. Substituting,

$$\dot{\mathbf{q}} = \lim_{h \rightarrow 0} \frac{(I + \delta \mathbf{q} / 2) \mathbf{q}(t) - \mathbf{q}(t)}{h} = \frac{1}{2} \omega \mathbf{q}. \quad (33)$$

Noting that in grid coordinates the angular velocity is $\Omega = \mathbf{q}^* \omega \mathbf{q}$, we finally obtain [47]⁵

$$\dot{\mathbf{q}} = \frac{1}{2} \mathbf{q} \Omega. \quad (34)$$

⁵ This reference uses the opposite convention of the one adapted here: Ω is the angular velocity in the fixed frame whereas ω is the angular velocity in the rotating frame.

3. Quaternion control system

The goal of the sector of the control-system for rotations is to keep the vector \vec{X} parallel to the vector \vec{C} . The misalignment between them can be measured by the rotation needed to make these vectors parallel:

$$\vec{Q}_R = \frac{\vec{C} \times \vec{X}}{\|\vec{C}\|^2}, \quad (35)$$

where the subscript ‘R’ indicates that this quantity is of relevance for rotations.⁶ The control-system needs to adjust the angular velocity $\vec{\Omega}$ such that $\vec{Q}_R \approx 0$. As long as the control-system works, this instantaneous rotation is small, and therefore, non-commutativity of rotations can be neglected. This suggests to control the angular velocity in the moving frame $\vec{\Omega}$ based on the control-parameter \vec{Q}_R .

We proceed as follows: We measure \vec{Q}_R regularly during the BBH evolution, and compute its first and second time-derivatives. As in earlier work [43] (and in many papers since [33–36, 38, 39, 44]), we use this to reset the third time-derivative of the mapping-parameters that determine the rotation. These parameters are the second time-derivative of $\vec{\Omega}(t)$; thus, we choose $\vec{\Omega}(t)$ such that it has constant second time-derivative. We periodically reset this constant using the equation

$$\frac{d^2\vec{\Omega}}{dt^2} = \alpha\vec{Q}_R + \beta\frac{d\vec{Q}_R}{dt} + \gamma\frac{d^2\vec{Q}_R}{dt^2}. \quad (36)$$

A constant value of $d^2\vec{\Omega}/dt^2$ implies that $\Omega(t)$ is a piecewise quadratic polynomial. Whenever the second derivative is reset, we choose integration constants such that $\vec{\Omega}$ and $d\vec{\Omega}/dt$ are continuous. Finally, we use $\vec{\Omega}(t)$ to determine the actual rotation-matrix via Eq. (34).

There are alternative control-feedback equations to Eq. (36). Some of them are discussed in [40]. The details of the feedback equation do not influence the main focus of this paper which is how to represent rotations and control parameters.

In SpEC, Eq. (34) is integrated with a 5-th order Dormand-Prince time-stepper [48].

While Eq. (34) analytically preserves the unit-norm of \mathbf{q} , numerical integration will not identically preserve $|\mathbf{q}| = 1$. Therefore, the $\mathbf{q}(t)$ returned by the ODE-integrator is rescaled to unit-length, $\mathbf{q} \rightarrow \mathbf{q}/|\mathbf{q}|$ before it is used to construct rotations.

Whenever $d^2\vec{\Omega}/dt^2$ is reset via Eq. (36), \mathbf{q} of the ODE integrator is also rescaled to unit length.

Equation (35) can also be derived with the formal procedure introduced in Section II B. This derivation will highlight an ambiguity not visible in Eq. (35), and will also result in the control parameters for scaling and translation. We start with

$$\bar{x} = a \mathbf{q} \mathbf{x} \mathbf{q}^* + \mathbf{T} \quad (37)$$

where $\bar{x}, \mathbf{x}, \mathbf{q}, \mathbf{T}$ are quaternions and $a \in \mathbb{R}$. All vector quantities are now treated as quaternions via the identification map $\mathbf{v} = (0, \vec{v})$. We now perturb $a \rightarrow a + \delta a$, $\mathbf{T} \rightarrow \mathbf{T} + \delta \mathbf{T}$, $\mathbf{q} \rightarrow \mathbf{q} \left(1 + \frac{\delta \mathbf{q}}{2}\right)$. The \mathbf{q} -perturbation will result in vectors \vec{v} being mapped to

$$\mathbf{v}' = \mathbf{q} \left(1 + \frac{\delta \mathbf{q}}{2}\right) \mathbf{v} \left(1 - \frac{\delta \mathbf{q}}{2}\right) \mathbf{q}^* = \mathbf{q} \mathbf{w} \mathbf{q}^* \quad (38)$$

where $\mathbf{w} \equiv \left(1 + \frac{\delta \mathbf{q}}{2}\right) \mathbf{v} \left(1 - \frac{\delta \mathbf{q}}{2}\right)$. This shows that the imaginary part $\vec{\delta q}$ of $\delta \mathbf{q} = (0, \vec{\delta q})$ represents a rotation in *grid* coordinates.

The quaternion version of Eq. (9) is:

$$a \mathbf{q} \mathbf{x}_i \mathbf{q}^* + \mathbf{T} = (a + \delta a) \mathbf{q} \left(1 + \frac{\delta \mathbf{q}}{2}\right) \mathbf{c}_i \left(1 - \frac{\delta \mathbf{q}}{2}\right) \mathbf{q}^* + \mathbf{T} + \delta \mathbf{T}. \quad (39)$$

with $i = A, B$. Because the real part of Eqs. (39) are trivially satisfied, Eqs. (39) represent six equations, three each for black hole A and for black hole B. We seek to solve Eqs. (39) for the unknowns δa , $\delta \mathbf{T} = (0, \vec{\delta T})$, and $\delta \mathbf{q} = (0, \vec{\delta q})$. Because $\delta \mathbf{T}$ and $\delta \mathbf{q}$ have three components each, we have in total seven unknowns. The additional degree of freedom arises because the rotation around \vec{C} is not yet fixed. Recall that in the Euler angle representation, we remove this degree of freedom by setting $\phi = 0$, c.f. Eq. (7). Expanding Eq. (39) to linear order in the perturbations and subtracting the equation for black hole B from that for black hole A, it is straightforward to show that

$$\delta a = \left(\frac{\vec{X} \cdot \vec{C}}{\|\vec{C}\|^2} - 1 \right) a, \quad (40)$$

$$\vec{\delta q} = \frac{\vec{C} \times \vec{X}}{\|\vec{C}\|^2} + \alpha \vec{C}, \quad (41)$$

and

$$(0, \vec{\delta T}) = a \mathbf{q} \left(\mathbf{x}_A - \mathbf{c}_A - \delta \mathbf{q} \wedge \mathbf{c}_A - \frac{\delta a}{a} \mathbf{c}_A \right) \mathbf{q}^*. \quad (42)$$

In Eq. (42), $\delta \mathbf{q} \wedge \mathbf{c}_A \equiv (0, \vec{\delta q} \times \vec{c}_A)$ and $\delta \mathbf{q}$, δa are to be substituted from Eq. (40, 41). The parameter α in Eq. (41) is undetermined, reflecting the extra degree of freedom already mentioned after Eq. (39). It parameterizes the component of $\vec{\delta q}$ parallel to \vec{C} ; i.e., a rotation

⁶ The normalization chosen corresponds to the fact that only the direction of the two vectors matter in the context of rotations, and due to the scaling control system we should have to first order, $\|\vec{X}\| \simeq \|\vec{C}\|$.

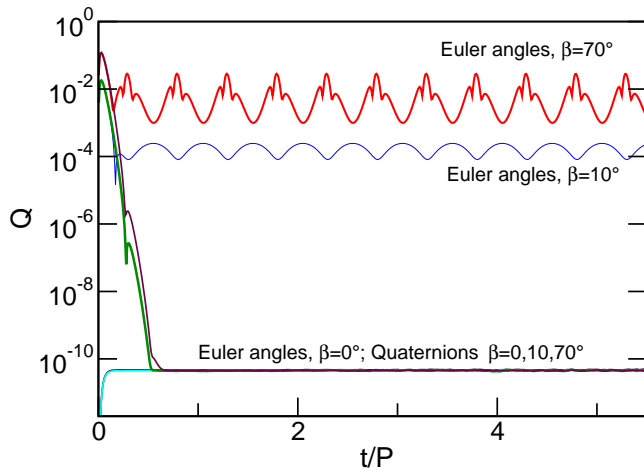


FIG. 2. Newtonian simulations with inclination of the orbital plane of angle $\beta = 0, 10, 70$ degrees from the xy plane, performed with both control systems. Time is measured in units of orbital period.

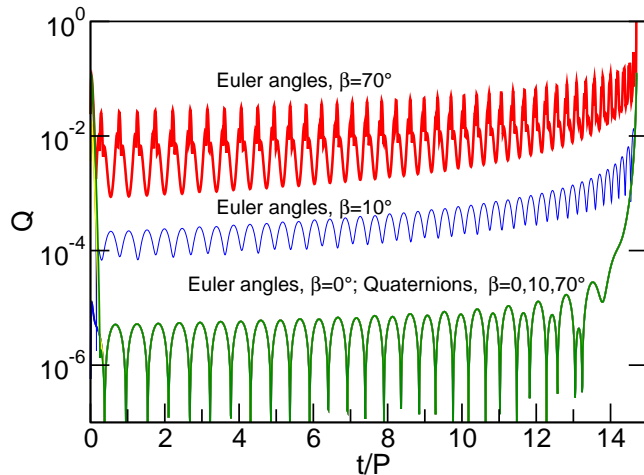


FIG. 3. Post-Newtonian simulations with inclination of the orbital plane angle $\beta = 0, 10, 70$ degrees from the $x - y$ plane, performed with both control systems. Time is measured in units of initial orbital period. The binary is equal mass and non-spinning, with the initial coordinate separation of 20.

about the axis \vec{C} connecting the two excision spheres. We shall choose it to minimize the overall rotation $\|\delta\vec{q}\|$:

$$\alpha = 0. \quad (43)$$

With this choice Eq. (41) simplifies to Eq. (35). The choice $\alpha = 0$ is equivalent to the minimal rotation frame of Boyle et al. [49]; it minimizes artificial activity of the control system that is not connected to the physics of the binary black hole.

III. NUMERICAL RESULTS

To test our new approach to the rotation control system we begin with the simplest possible system that still exhibits the desired behaviour, namely a *Newtonian* circular binary. We consider an equal mass, non-spinning, circular binary at separation of $20 M$. The orbital plane is inclined with respect to the xy -plane by angles $\beta = 0, 10, 70$ degrees. The performance of the control system is quantified by the magnitude of the control parameters $\|Q\| \equiv \sqrt{Q_i Q^i}$ where the summation extends over all the components of the control error for rotation, defined by Eqs. (10b, 10c) for Euler angles and Eq. (41) for quaternions. Independent of the inclination β , we always initialize the control system as if the binary is in the xy -plane. This is of course only correct for $\beta = 0$; for $\beta \neq 0$, the control system will also have to demonstrate that it can compensate for an utterly erroneous initialization. Figure 2 shows $\|Q\|$ for the 3 cases. For $\beta = 0^\circ$ both control systems perform very well with an extremely small value of $Q \sim 10^{-11}$. For $\beta \neq 0$, there are initial transients due to the intentionally wrong initialization of λ^μ . These transients decay exponentially on the damping timescale of the control system; here, $\tau = P/56$ where P is the orbital period. Once the transients have disappeared for $\beta = 10^\circ$, the quaternion results are unchanged while the Euler-angle control error has increased by 6 orders of magnitude. Several periodic sharp features start to appear. Finally, for $\beta = 70^\circ$ the quaternion $\|Q\|$ is again at 10^{-11} while the Euler-angle $\|Q\|$ grows by another two orders of magnitude and shows sharp oscillatory features, which ultimately makes the control system inviable.

Figure 2 foreshadows already the main conclusion of this work: The Euler-angle approach depends on the plane of the orbit, and has increasing difficulty in controlling the coordinate mappings as the orbital plane becomes orthogonal to the xy -plane. While the Euler-angle control system becomes singular only at exactly $\beta = 90^\circ$, the effects of this singularity are already clearly visible for $\beta = 10^\circ$. In contrast, the quaternion control system is rotationally invariant, and hence, it controls the coordinate mapping equally well for any inclination β .

Next, we turn to a more interesting test that also involves the control system for the expansion factor $a(t)$. We consider a post-Newtonian equal mass, non-spinning black hole binary. The relevant PN equations of motion can be found in [50]. Figure 3 displays a set of three runs done with both control systems, again choosing to tilt the orbit relative to the xy -plane by angles $\beta = 0, 10, 70$ degrees.

After the initial transients due to intentionally wrong initialization of the control system, both of the control systems handle the $\beta = 0$ case equally well with $\|Q\| \sim 10^{-5}$ showing regular oscillations due to a small eccentricity of the orbit. When $\beta = 10^\circ$, the quaternion control system performs in exactly the same fashion as for $\beta = 0^\circ$. The Euler-angle system, on the other hand,

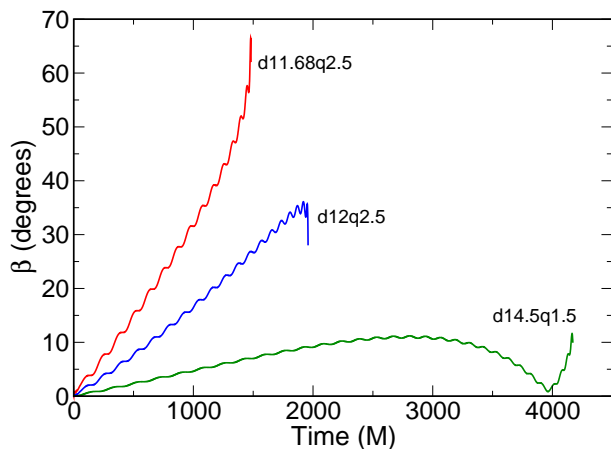


FIG. 4. The inclination angle, β for the three systems under study.

begins to struggle: the amplitude of $\|Q\|$ grows by about two orders of magnitude. The situation grows worse still for Euler angles when $\beta = 70^\circ$, where the control error increases by another two orders of magnitude and sharp features appear.

Meanwhile, the curves corresponding to the quaternion control system show exactly (to within numerical accuracy) the same value of $\|Q\|$ for all inclinations. This is exactly what we expect from a rotationally invariant control system - the orientation of the orbital plane is irrelevant.

Finally, we test the quaternion-based control system using its main application: simulations of precessing binary black hole systems in full numerical relativity. Quite generally, this precession may cause the orbital plane to rotate by 90 or more degrees with respect to the initial conditions. The behaviour of the system depends on mass ratio and the two spin vectors. We choose a set of three simulations to be evolved using full numerical relativity that exhibits mild to significant precession. Table I summarizes the initial conditions. The initial data was constructed from the superposition of two Kerr-Schild metrics for the conformal metric as in [51] (so called SKS initial data). The eccentricity has been removed by an iterative process [52], so that the final eccentricities for all three cases are a few $\times 10^{-4}$.

Figure 4 shows the inclination angle $\beta \equiv \arccos(\Omega_z/|\vec{\Omega}|)$ which measures the angle between the normal to the instantaneous orbital plane and the initial direction of the normal, which is by convention in the z -direction. The high-frequency oscillatory features are due to the nutation of the orbital angular momentum, while the secular evolution is due to precession. Notice that the d14.5q1.5 run completes a full precession cycle at $t = 4000M$. The curves end when the black holes merge. The maximum inclination angles are similar to those used for the Post-Newtonian evolutions above. Figure 5 shows the trajectories of the black holes in inertial coordinates.

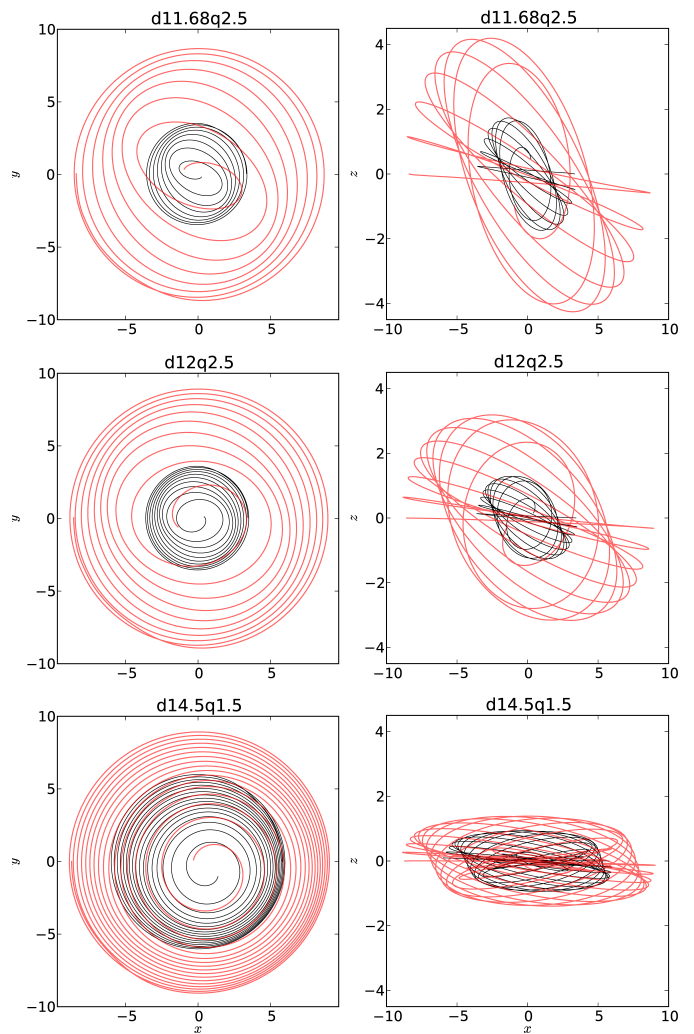


FIG. 5. The trajectories of the centers of the apparent horizons of the black holes in inertial coordinates for the 3 simulations. Top to bottom: d11.68q2.5, d12q2.5, d14.5q1.5. The left panels show the projection onto the xy plane and the right, the xz plane

Figure 6 presents $\|Q\|$ for the three runs done with the quaternion control system. In the main panel of Figure 6 it is difficult to compare the $\|Q\|$ of different runs because of the difference in orbital frequency. The inset shows the same $\|Q\|$ residuals for the three simulations but timeshifted such that the orbital frequency of $M\Omega = 0.025$ occurs at $t = 0$. As one can see the control error norms lie very close to each other, and exhibit qualitatively similar oscillations with virtually no sharp features. The remaining differences in behaviour are associated mostly with the different eccentricities as well as masses and spins. The growth of the control parameters with time is caused by the more rapid inspiral towards merger. Our numerical experiments demonstrate that the quaternion approach is indeed suitable for simulating arbitrarily precessing configurations.

Name	q	$\vec{\chi}_1$	$\vec{\chi}_2$	D_0/M	\dot{a}_0	$M\Omega_0$
d11.68q2.5	2.5	(0.000, 0.575, -0.556)	(0.000, 0.360, -0.347)	11.68	-0.000290589649	0.02264246
d12q2.5	2.5	(0.000, 0.410, -0.287)	(0, 0, 0)	12	-0.000108923113	0.02180603
d14.5q1.5	1.5	(0.000, 0.285, 0.093)	(0, 0, 0)	14.5	-0.000016947638	0.01664958

TABLE I. The initial conditions used for the numerical relativity runs. Given are the mass ratio $q = m_1/m_2$, the dimensionless spin-vectors $\vec{\chi}_1$ and $\vec{\chi}_2$, the initial separation D_0 , initial radial velocity \dot{a}_0 , initial orbital frequency Ω_0 . The initial orbital angular momentum is in the \hat{z} direction and the line connecting the two black holes is parallel to the x -axis.

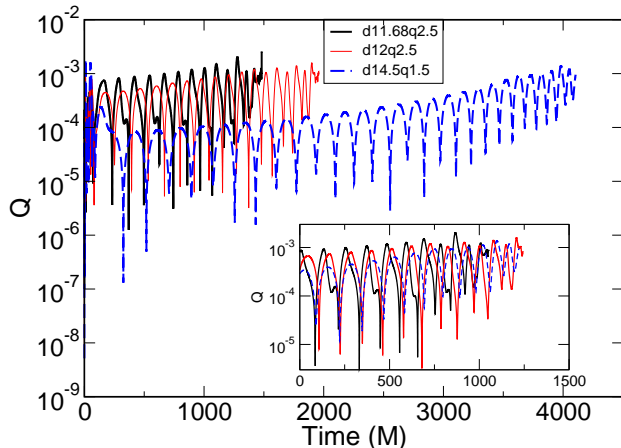


FIG. 6. Three full NR simulations performed with the quaternion control systems. The initial conditions are listed in Table I

IV. DISCUSSION

Simulating precessing binaries poses a challenge for excision-based numerical techniques. This challenge is resolved here by developing coordinate mappings which make the black holes be at rest in grid coordinates. This transformation is dynamically controlled by a feedback control system since the trajectories of the black holes are not known in advance. In the most general case this map involves a rotation, and while Euler angle parametrization works well for mildly precessing binaries, it exhibits coordinate singularities for polar orbits which leads to the breakdown of the simulation. To rectify the situation, we have created a control system that represents rotations using quaternions. Quaternions do not suffer from coordinate singularities and work for generically precessing systems. The quaternion-based control system is able to successfully perform fully general relativistic simulations of highly-precessing binaries, allowing the investigation strongly precessing binary black holes and broadening the range of parameter space that can be explored. The techniques developed here have already been utilized in the simulations presented in [41, 42]

The quaternion control system, as described and developed above, is related to the minimal rotation frame [49] (see also [53]). For the control-system developed here, as in the minimal rotation frame, a preferred *axis* exists (the line connecting the two black holes vs. the instantaneous

preferred emission axis of the gravitational waves). In both cases, the rotation *about* this axis is not a priori determined. And in both cases, this rotation is chosen such that the instantaneous rotation frequency of the rotating frame is minimal. In the present context, this condition is imposed by Eq. (43).

As a useful byproduct of the quaternion control system, one obtains an accurate estimate of the orbital frequency and the orbital phase during the numerical run without the need for any post-processing. The Ω in Eq. (34) is the instantaneous rotation frequency of the grid frame relative to the inertial frame, given in components of the grid frame. Converting to the inertial frame,

$$(0, \vec{\omega}) = \mathbf{q}\Omega\mathbf{q}^*. \quad (44)$$

If the control system were perfect - i.e. if $Q \equiv 0$ - then $\vec{\omega}$ given by Eq. (44) would be the instantaneous orbital frequency. Because $Q \neq 0$, Eq. (44) only gives an approximate orbital frequency, albeit a very good one: The upper panel of Fig. 7 shows the fractional difference between $|\vec{\omega}|$ from Eq. (44) and the exact numerical orbital frequency obtained by post-processing. The difference oscillates around zero with relative amplitude of 1×10^{-3} . It is also straightforward to integrate

$$\dot{\phi} = |\vec{\Omega}| = |\vec{\omega}| \quad (45)$$

to obtain the orbital phase of the precessing binary. In practice, we add Eq. (45) to the set of ordinary differential equations Eq. (34) that are integrated to obtain the rotation quaternion $\mathbf{q}(t)$. The difference between the orbital phase from the control system Eq. (45) and the exact orbital phase from the BH trajectories is shown in the lower panel of Fig. 7. The difference is $\sim 10^{-4}$ radians until merger, during an inspiral lasting 105 radians. Incidentally, this again demonstrates that our control system works exactly as expected.

ACKNOWLEDGMENTS

We thank Mark Scheel for assistance in implementing the quaternion control system in SpEC, and Mark Scheel and Bela Szilagyi for assistance with running the mergers of the black hole binaries discussed in Sec. III. We gratefully acknowledge support from NSERC of Canada,

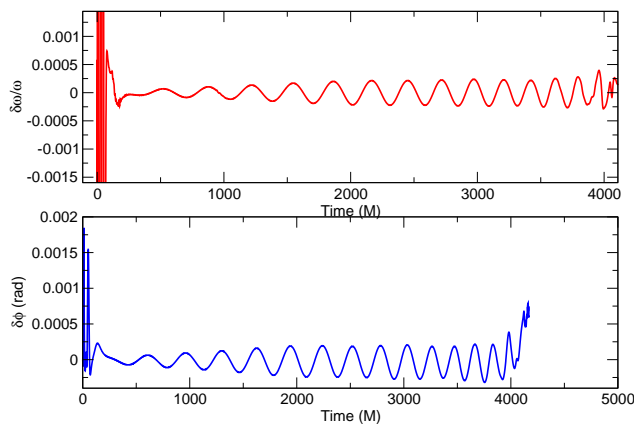


FIG. 7. Top: the fractional difference in orbital frequency estimated from quaternions and from trajectories. Bottom: the orbital phase difference in radians. The data is from the run d14.5q1.5

from the Canada Research Chairs Program, and from the Canadian Institute for Advanced Research. We further gratefully acknowledge support from the Sherman Fairchild Foundation, NSF Grants No. PHY-0969111 and No. PHY-1005426 and NASA Grant No. NNX09AF96G at Cornell. Calculations were performed at the GPC supercomputer at the SciNet HPC Consortium; SciNet is funded by: the Canada Foundation for Innovation (CFI) under the auspices of Compute Canada; the Government of Ontario; Ontario Research Fund (ORF) – Research Excellence; and the University of Toronto. Further computations were performed on the Caltech compute cluster Zwicky, which was funded by the Sherman Fairchild Foundation and the NSF MRI-R2 grant No. PHY-0960291, and on the Gravity compute cluster funded by CFI, ORF, and the University of Toronto.

APPENDIX

A. Rotation control parameters in matrix notation

The underlying idea for the rotational control system that we have described in section II C 3 is independent of the use of quaternions to represent rotations. For example, one could have used infinitesimal rotation matrices to achieve the same goal. Below is the demonstration of the same derivation as in section II C 3 but now in terms of a rotation matrix R . We start with the following version of Eq. (9):

$$aR\vec{x}_i + \vec{T} = (a + \delta a)R(I + \delta R)\vec{c}_i + \vec{T} + \delta\vec{T} \quad (46)$$

where as usual $i = A, B$, $\vec{x}_i, \vec{c}_i, \vec{T}, \delta\vec{T} \in \mathbb{R}^3$, I is the identity matrix, $a, \delta a \in \mathbb{R}$ and $R, \delta R \in M_{3 \times 3}$. Once more we seek to solve this system of six equations for the unknowns $\delta a, \delta\vec{T}$, and δR . Note that since δR is an infinitesimal rotation matrix, it is skew symmetric and thus has three independent components, for a total of seven unknowns. Expanding Eq. (46) to first order in perturbation and subtracting the equation for black hole B from that of black hole A one can show that:

$$\delta a = \left(\frac{\vec{X} \cdot \vec{C}}{\|\vec{C}\|^2} - 1 \right) a, \quad (47)$$

$$\delta R_{ij} = \epsilon_{ijk} \delta\phi^j, \quad \delta\vec{\phi} = \frac{\vec{C} \times \vec{X}}{\|\vec{C}\|^2} + a\vec{C}, \quad (48)$$

$$\delta\vec{T} = aR \left(\vec{x}_A - \vec{c}_A - \delta\vec{\phi} \times \vec{c}_A - \frac{\delta a}{a} \vec{c}_A \right). \quad (49)$$

These results match exactly Eqs. (40)-(42). Thus we see that indeed infinitesimal rotation matrices could have been used to represent rotation. We selected quaternions for our work primarily for numerical reasons, the main being the ease of correcting numerical drift from a rotation, which for quaternions amounts to a simple renormalization.

[1] J. Aasi *et al.* (LIGO Scientific Collaboration, Virgo Collaboration), (2013), arXiv:1304.0670 [gr-qc].
 [2] J. Abadie *et al.* (LIGO Scientific), *Class. Quant. Grav.* **27**, 173001 (2010), arXiv:1003.2480 [Unknown].
 [3] L. S. Finn, *Phys. Rev. D* **46**, 5236 (1992).
 [4] L. S. Finn and D. F. Chernoff, *Phys. Rev. D* **47**, 2198 (1993).
 [5] F. Ohme, *Class.Quant.Grav.* **29**, 124002 (2012), arXiv:1111.3737 [gr-qc].

[6] F. Pretorius, *Phys.Rev.Lett.* **95**, 121101 (2005), arXiv:gr-qc/0507014 [gr-qc].
 [7] I. Hinder, *Class. Quant. Grav.* **27**, 114004 (2010), arXiv:1001.5161 [gr-qc].
 [8] H. P. Pfeiffer, *Class.Quant.Grav.* **29**, 124004 (2012), arXiv:1203.5166 [gr-qc].
 [9] L. Blanchet, *Living Reviews in Relativity* **5** (2002).
 [10] L. Blanchet, *Fundam.Theor.Phys.* **162**, 125 (2011), arXiv:0907.3596 [gr-qc].
 [11] A. Buonanno and T. Damour, *Phys.Rev.* **D59**, 084006 (1999),

- arXiv:gr-qc/9811091 [gr-qc].
- [12] T. Damour, Phys.Rev. **D64**, 124013 (2001), arXiv:gr-qc/0103018 [gr-qc].
- [13] T. Damour, B. R. Iyer, and A. Nagar, Phys.Rev. **D79**, 064004 (2009), arXiv:0811.2069 [gr-qc].
- [14] T. Damour, (2012), arXiv:1212.3169 [gr-qc].
- [15] T. Damour and A. Nagar, Phys. Rev. D **79**, 081503 (2009), arXiv:0902.0136 [gr-qc].
- [16] A. Buonanno, Y. Pan, H. P. Pfeiffer, M. A. Scheel, L. T. Buchman, *et al.*, Phys. Rev. D **79**, 124028 (2009), arXiv:0902.0790 [gr-qc].
- [17] A. Taracchini, A. Buonanno, E. Barausse, M. Boyle, T. Chu, G. Lovelace, H. P. Pfeiffer, and M. A. Scheel, Phys.Rev. **D83**, 104034 (2012), arXiv:1202.0790 [gr-qc].
- [18] T. A. Apostolatos, C. Cutler, G. J. Sussman, and K. S. Thorne, Phys. Rev. D **49**, 6274 (1994).
- [19] M. Campanelli, C. O. Lousto, Y. Zlochower, B. Krishnan, and D. Merritt, Phys. Rev. D **75**, 064030 (2007), gr-qc/0612076.
- [20] M. Campanelli, C. O. Lousto, H. Nakano, and Y. Zlochower, Phys. Rev. D **79**, 084010 (2009), arXiv:gr-qc/0808.0713.
- [21] R. Sturani, S. Fischetti, L. Cadonati, G. Guidi, J. Healy, *et al.*, (2010), arXiv:1012.5172 [gr-qc].
- [22] R. Sturani, S. Fischetti, L. Cadonati, G. Guidi, J. Healy, *et al.*, J.Phys.Conf.Ser. **243**, 012007 (2010), arXiv:1005.0551 [gr-qc].
- [23] P. Schmidt, M. Hannam, S. Husa, and P. Ajith, Phys. Rev. D **84**, 024046 (2011), arXiv:1012.2879.
- [24] Y. Zlochower, M. Campanelli, and C. O. Lousto, Class.Quant.Grav. **28**, 114015 (2011), arXiv:1011.2210 [gr-qc].
- [25] C. O. Lousto and Y. Zlochower, Phys.Rev.Lett. **107**, 231102 (2011), arXiv:1108.2009 [gr-qc].
- [26] C. O. Lousto and Y. Zlochower, (2012), arXiv:1211.7099 [gr-qc].
- [27] T. Damour, A. Nagar, and M. Trias, Phys. Rev. D **83**, 024006 (2011), arXiv:1009.5998 [gr-qc].
- [28] L. Santamaría, F. Ohme, P. Ajith, B. Brügmann, N. Dorband, M. Hannam, S. Husa, P. Mösta, D. Pollney, C. Reisswig, E. L. Robinson, J. Seiler, and B. Krishnan, Phys. Rev. D **82**, 064016 (2010), arXiv:1005.3306 [gr-qc].
- [29] M. Boyle, Phys. Rev. D **84**, 064013 (2011).
- [30] F. Ohme, M. Hannam, and S. Husa, Phys. Rev. D **84**, 064029 (2011).
- [31] I. MacDonald, A. H. Mroue, H. P. Pfeiffer, M. Boyle, L. E. Kidder, *et al.*, (2012), arXiv:1210.3007 [gr-qc].
- [32] <http://www.black-holes.org/SpEC.html>.
- [33] M. Boyle, D. A. Brown, L. E. Kidder, A. H. Mroué, H. P. Pfeiffer, M. A. Scheel, G. B. Cook, and S. A. Teukolsky, Phys. Rev. D **76**, 124038 (2007).
- [34] M. A. Scheel, M. Boyle, T. Chu, L. E. Kidder, K. D. Matthews and H. P. Pfeiffer, Phys. Rev. D **79**, 024003 (2009), arXiv:gr-qc/0810.1767.
- [35] T. Chu, H. P. Pfeiffer, and M. A. Scheel, Phys. Rev. D **80**, 124051 (2009), arXiv:0909.1313 [gr-qc].
- [36] L. T. Buchman, H. P. Pfeiffer, M. A. Scheel, and B. Szilagyi, Phys. Rev. D **86**, 084033 (2012), arXiv:1206.3015 [gr-qc].
- [37] G. Lovelace, M. Boyle, M. A. Scheel, and B. Szilágyi, Class. Quant. Grav. **29**, 045003 (2012), arXiv:arXiv:1110.2229 [gr-qc].
- [38] G. Lovelace, M. A. Scheel, and B. Szilágyi, Phys. Rev. D **83**, 024010 (2011), arXiv:1010.2777 [gr-qc].
- [39] A. H. Mroue and H. P. Pfeiffer, (2012), arXiv:1210.2958 [gr-qc].
- [40] D. A. Hemberger, M. A. Scheel, L. E. Kidder, B. Szilagyi, and S. A. Teukolsky, (2012), arXiv:1211.6079 [gr-qc].
- [41] F. Foucart, M. B. Deaton, M. D. Duez, L. E. Kidder, I. MacDonald, C. D. Ott, H. P. Pfeiffer, M. A. Scheel, B. Szilagyi, and S. A. Teukolsky, Phys. Rev. D **87**, 084006 (2013).
- [42] A. H. Mroué, M. A. Scheel, B. Szilágyi, H. P. Pfeiffer, M. Boyle, D. A. Hemberger, L. E. Kidder, G. Lovelace, S. Ossokine, N. W. Taylor, A. I Zenginoğlu, L. T. Buchman, T. Chu, M. Giesler, R. Owen, and S. A. Teukolsky, in preparation (2013).
- [43] M. A. Scheel, H. P. Pfeiffer, L. Lindblom, L. E. Kidder, O. Rinne, and S. A. Teukolsky, Phys. Rev. D **74**, 104006 (2006).
- [44] H. P. Pfeiffer, D. A. Brown, L. E. Kidder, L. Lindblom, G. Lovelace, and M. A. Scheel, Class. Quantum Grav. **24**, S59 (2007), gr-qc/0702106.
- [45] B. Szilagyi, L. Lindblom, and M. A. Scheel, Phys. Rev. D **80**, 124010 (2009), arXiv:0909.3557 [gr-qc].
- [46] S. Altmann, *Rotations, quaternions, and double groups* (Dover Publications, Mineola, N.Y., 2005).
- [47] M. Arribas, A. Elipe, and M. Palacios, Celestial Mechanics and Dynamical Astronomy **96**, 239 (2006).
- [48] W. H. Press, S. A. Teukolsky, W. T. Vetterling, and B. P. Flannery, *Numerical Recipes: The Art of Scientific Computing (3rd Ed.)* (Cambridge University Press, New York, 2007).
- [49] M. Boyle, R. Owen, and H. P. Pfeiffer, Phys. Rev. D **84**, 124011 (2011), arXiv:1110.2965 [gr-qc].
- [50] L. E. Kidder, Phys. Rev. D **52**, 821 (1995).
- [51] G. Lovelace, R. Owen, H. P. Pfeiffer, and T. Chu, Phys. Rev. D **78**, 084017 (2008).
- [52] A. Buonanno, L. E. Kidder, A. H. Mroué, H. P. Pfeiffer, and A. Taracchini, Phys.Rev. **D83**, 104034 (2011), arXiv:1012.1549 [gr-qc].
- [53] A. Buonanno, Y. Chen, and M. Vallisneri, Phys. Rev. D **67**, 104025 (2003), arXiv:gr-qc/0211087 [gr-qc].